

# **$^{18}\text{F}$ -FLT PET as a Surrogate Marker of Drug Efficacy During mTOR Inhibition by Everolimus in a Preclinical Cisplatin-Resistant Ovarian Tumor Model**

Nicolas Aide<sup>1-3</sup>, Kathryn Kinross<sup>3,4</sup>, Carleen Cullinane<sup>4</sup>, Peter Roselt<sup>3</sup>, Kelly Waldeck<sup>4</sup>, Oliver Neels<sup>3</sup>, Donna Dorow<sup>3,4</sup>, Grant McArthur<sup>3-5</sup>, and Rodney J. Hicks<sup>3,5</sup>

<sup>1</sup>Bioticla Team, EA1772, IFR 146 ICORE, GRECAN, François Baclesse Cancer Centre and Caen University, Caen, France; <sup>2</sup>PET Unit, Caen University Hospital and François Baclesse Cancer Centre, Caen, France; <sup>3</sup>Centre for Molecular Imaging and Translational Research Laboratory, Peter MacCallum Cancer Centre, East Melbourne, Australia; <sup>4</sup>Sir Donald and Lady Trespowthick Laboratories, Peter MacCallum Cancer Centre, East Melbourne, Australia; and <sup>5</sup>Department of Medicine, University of Melbourne, Parkville, Australia

Targeting the mammalian target of rapamycin (mTOR) pathway is a potential means of overcoming cisplatin resistance in ovarian cancer patients. Because mTOR inhibition affects cell proliferation, we aimed to study whether 3'-deoxy-3'- $^{18}\text{F}$ -fluorothymidine ( $^{18}\text{F}$ -FLT) PET could be useful for monitoring early response to treatment with mTOR inhibitors in an animal model of cisplatin-resistant ovarian tumor. **Methods:** BALB/c nude mice bearing subcutaneous human SKOV3 ovarian cancer xenografts were treated with either the mTOR inhibitor everolimus (5 mg/kg) or vehicle, and  $^{18}\text{F}$ -FLT PET was performed at baseline, day 2, and day 7 of treatment.  $^{18}\text{F}$ -FLT uptake was evaluated by calculation of mean standardized uptake value (SUVmean) corrected for partial-volume effect. Ex vivo immunohistochemistry studies were performed on separate cohorts of mice treated as above and sacrificed at the same time points as for the PET studies. The ex vivo analysis included bromodeoxyuridine incorporation as a marker of cell proliferation, and phosphorylation of ribosomal protein S6 as a downstream marker of mTOR activation. **Results:** During the treatment period, no significant change in tumor  $^{18}\text{F}$ -FLT uptake was observed in the vehicle group, whereas in everolimus-treated mice,  $^{18}\text{F}$ -FLT SUVmean decreased by 33% ( $P = 0.003$ ) at day 2 and 66% ( $P < 0.001$ ) at day 7, compared with baseline. Notably, the reduction of  $^{18}\text{F}$ -FLT uptake observed at day 2 in the everolimus group preceded changes in tumor volume, and a significant difference in  $^{18}\text{F}$ -FLT uptake was observed between vehicle and drug-treated tumors at both day 2 ( $P = 0.0008$ ) and day 7 ( $P = 0.01$ ). In ex vivo studies, everolimus treatment resulted in a 98% reduction in phosphorylated ribosomal protein S6 immunostaining at day 2 ( $P = 0.02$ ) and 91% reduction at day 7 ( $P = 0.003$ ), compared with the vehicle group. Bromodeoxyuridine incorporation was reduced by 65% at day 2 (not significant) and by 41% at day 7 ( $P = 0.02$ ) in drug versus vehicle groups. **Conclusion:** Reduction in  $^{18}\text{F}$ -FLT uptake correlates well with the level of mTOR inhibition by everolimus in the SKOV3 ovarian tumor model. These data suggest that early treatment monitoring by  $^{18}\text{F}$ -FLT PET may be of use in future

preclinical or clinical trials evaluating treatment of cisplatin-resistant ovarian tumors by mTOR inhibitors.

**Key Words:** animal imaging; oncology; PET; FLT; mTOR inhibition; ovarian cancer; small-animal PET

**J Nucl Med 2010; 51:1559–1564**

DOI: 10.2967/jnumed.109.073288

Ovarian cancer is the leading cause of death among gynecologic cancers, because disease has often already disseminated to the peritoneal cavity and lymph node stations at diagnosis. Despite optimal treatment, including debulking surgery and adjuvant or neoadjuvant chemotherapy with a platinum–paclitaxel combination, which yield response rates of over 80%, most of the patients will eventually relapse (1). The issue of platinum resistance may arise at the first relapse or later in the course of the disease, but the response rate to chemotherapy regimens will decrease at each subsequent relapse. There is therefore a need for new therapeutic strategies including molecularly targeted therapies to overcome this chemoresistance (2).

The phosphoinositide-3-kinase/AKT signaling pathway may be a potential target, because AKT regulates various cellular pathways promoting cell survival, cell proliferation, angiogenesis, and invasion. Among the downstream effectors of AKT is the mammalian target of rapamycin (mTOR) (3), which is inhibited by several molecules including rapamycin, temsirolimus (CCI-779; Wyeth) (4,5), and everolimus (RAD001; Novartis) (6). Everolimus has been shown to inhibit human ovarian cancer cell proliferation and to enhance the effect of cisplatin in vivo in an ovarian cancer xenograft model (7). Also, everolimus has been shown to delay tumor onset and progression in a transgenic mouse model of ovarian carcinoma (8).

PET imaging has been shown to be particularly useful for evaluating the efficacy of molecularly targeted therapies given either alone or in combination with conventional chemotherapies in preclinical studies (9,10). In clinical

Received Jan. 25, 2010; revision accepted Mar. 24, 2010.

For correspondence or reprints contact: Nicolas Aide, Nuclear Medicine Department, Centre François Baclesse, Avenue Général Harris, 14076 Caen Cedex 5, France.

E-mail: [n.aide@baclesse.fr](mailto:n.aide@baclesse.fr)

COPYRIGHT © 2010 by the Society of Nuclear Medicine, Inc.

trials, PET can predict metabolic changes before tumor shrinkage, at a time when conventional imaging modalities and conventional criteria of evaluation (the criteria of the World Health Organization or the response evaluation criteria in solid tumors) are ineffective (11). PET may also be particularly useful in the field of molecularly targeted therapies, which often have a cytostatic effect.

The aim of the present study was to evaluate the ability of 3'-deoxy-3'-<sup>18</sup>F-fluorothymidine (<sup>18</sup>F-FLT), a PET probe for cell proliferation (12), to predict early response to everolimus in a mouse model of subcutaneously transplanted human cisplatin-resistant ovarian cancer.

## MATERIALS AND METHODS

### Cell Line Culture

SKOV-3 cells (National Institutes of Health), a human clear cell carcinoma cell line that is resistant to cisplatin, were grown in RPMI medium supplemented with 10% fetal calf serum, 1% L-glutamine, and 1% penicillin/streptomycin.

### Animal Models

Six- to 10 wk-old nude mice (Animal Resources Centre) received a subcutaneous injection in the right hind limb of  $10 \times 10^6$  SKOV-3 cells in 0.05 mL of 50% RPMI/Matrigel (BD Bioscience). To improve the tumor uptake rate, we gave the animals a single 2.5-Gy dose of whole-body irradiation 24 h before cell implantation.

The animals were allowed to feed ad libitum. Experiments were performed in accordance with the National Health and Medical Research Council code of practice for the care and use of animals for scientific purposes and with approval from the Peter MacCallum Cancer Centre Animal Experimentation Ethics Committee. At 4 wk after implantation (tumor volume  $\approx 60 \text{ mm}^3$ ), tumor-bearing animals were randomized into 2 groups and drug treatment commenced. Tumor volumes were estimated using the formula (greatest diameter  $\times$  smallest diameter<sup>2</sup>)/2. The same experienced animal technician always performed caliper measurements.

### Drug Preparation

Everolimus emulsion (provided by Novartis) was diluted in 5% glucose and administered orally once daily at 0.1 mL/10 g of body weight. Control animals received placebo emulsion diluted in glucose as above.

### Study Design

Two cohorts of mice were used (Table 1). The first consisted of 14 mice (7 treated and 7 control), which were imaged by <sup>18</sup>F-FLT PET at baseline, 2 d, and 7 d after daily treatment with everolimus (treated group) or vehicle (control group). The second cohort (15 mice) was used for correlative immunohistochemistry studies, 3 mice being sacrificed for tumor harvesting at baseline and 3 each control and drug-treated animals sacrificed at days 2 and 7 of treatment.

### Tracer Production

<sup>18</sup>F-FLT was prepared on the Tracerlab FXFN module (GE Healthcare) using the method described by Machulla et al. (13). Tracer purity was controlled by high-performance liquid chromatography, and ethanol concentration was always kept below 7%.

### Small-Animal (SA) PET Examinations

SA PET examinations were performed on a Mosaic SA PET scanner (Philips). The resolution of this system is 2.7 mm at the

**TABLE 1.** Details of the Experimental Design

Study	Group	Day 0 (baseline)	Day 2	Day 7
SA PET	Control	7	7	5*
	Treated	7	7	7*
Correlative	Control	3 IHC	3 IHC	3 IHC
	Treated		3 IHC	3 IHC

IHC = immunohistochemistry studies.

\*In these animals, tumors were also harvested for immunohistochemistry studies.

center of the field of view (14). The energy window was 450–700 keV, and the coincidence-timing window was 6 ns. Data were acquired in 3-dimensional mode, corrected for decay and randoms. Acquisition time was 10 min per bed position. Reconstruction was performed with the 3-dimensional row-action maximum-likelihood algorithm (15). Attenuation correction was not applied.

SA PET calibration was performed as recommended by the manufacturer. Briefly, a 6-cm-diameter cylinder was filled with an <sup>18</sup>F-FDG solution of known activity. The cylinder was dynamically scanned (20 frames) overnight. A circular region of interest encompassing the entire cylinder diameter was drawn on 4 consecutive transverse planes at the middle of the cylinder. The calibration factor was obtained by dividing the known radioactivity in the cylinder (MBq/mL) by the image region of interest (counts/pixel/s).

Animals were kept fasting for 3 h and were injected intravenously with an average activity of 15 MBq of <sup>18</sup>F-FLT through a tail vein as described previously (10).

### Quantification of Tracer Uptake

Tumor activity was obtained from a volume of interest (VOI) encompassing the entire lesion. VOIs were determined by means of an isocontour, which was set so that the VOI matched the apparent tumor volume on PET. This kind of VOI is warranted when one wants to correlate tracer uptake with immunochemistry with whole-histologic-section quantification, in order to take into account tumor heterogeneity. Mean standardized uptake value (SUV<sub>mean</sub>) was computed according to the following formula:  $\text{SUV}_{\text{mean}} = (\text{tumor activity [Bq/mL]}) / (\text{injected activity [Bq/animal weight [g]]})$ , assuming a density of 1 g/cm<sup>3</sup>. Maximum standardized uptake value (SUV<sub>max</sub>) was also computed, using the same formula but with the maximum voxel value within the tumor VOI.

Because the use of VOI may lead to partial-volume effects (16), a correction for partial-volume effects was applied using recovery coefficients determined with a phantom study. A microDeluxe mouse-sized phantom (Data Spectrum Corp.) was used. This consisted of a cylinder (internal diameter, 4.5 cm; external diameter, 5 cm) containing fillable spheres. The fillable sphere diameters were 3.95, 4.95, 6.23, 7.86, and 9.89 mm, and their centers were on a single transaxial plane. Both cylinder and spheres were filled with an <sup>18</sup>F-FDG solution with a background activity of 0.46 MBq/mL and sphere-to-background ratios of 5 and 2.5. Recovery coefficients, defined as the ratio between measured and true activity (16), as used previously in SA PET phantom and rat imaging (9,17), were computed. Measured activity, expressed in Bq/mL, was obtained from a region of interest, which was drawn in a transverse plane according to the sphere dimensions. Plots of recovery coefficient against sphere diameters were obtained, and curves were then fitted to obtain recovery coefficient as a function

of sphere diameters. Radioactivity measurements on animal tumors were then corrected using the recovery coefficient values based on greatest tumor diameters, as measured by caliper the day of the SA PET examination.

### Immunohistochemistry

Each mouse received a 100 mg/kg intraperitoneal injection of bromodeoxyuridine (BrdU), and 1 h later the tumors were harvested, fixed in formalin, and embedded in paraffin. Sections (4  $\mu$ m) were stained for BrdU (catalog no. 347580; BD Biosciences) or phosphorylation of ribosomal protein S6 (pS6) (catalog no. 2211; Cell Signaling) using standard techniques in a Dako Auto-stainer, and sections were counterstained with hematoxylin. Quantification was performed using Meta Imaging series 7.6 software. For BrdU staining, 3 representative low-power images per section were analyzed for BrdU-positive cells, with the average positive cell count determined for the viable tumor. For pS6 staining, 3 representative low-power images per section were analyzed for integrated optical density (average intensity of positive staining per field) of areas of viable tumor (18).

### Statistical Analysis

Data are presented as mean  $\pm$  SD. The change in SUVmean over the different time points is reported as a percentage, compared with baseline, according to the following formula: change in SUVmean at day  $x$  = [(SUVmean at day  $x$  – SUVmean at baseline)/SUVmean at baseline]  $\times$  100. The change in BrdU or pS6 staining in the everolimus groups, compared with the vehicle group, at days 2 and 7 is defined as follows: [(mean immunohistochemistry quantitative value in everolimus group – mean immunohistochemistry quantitative value in vehicle group)/(mean immunohistochemistry quantitative value in vehicle group)]  $\times$  100.

The paired  $t$  test was used to compare tracer uptake in the same tumors over time, and the Student  $t$  test was used to compare tumor uptake, tumor volume, and immunohistochemistry quantitative data in the control and treated groups at specific time points. A 2-tailed  $P$  value of 0.05 or less was considered statistically significant. Statistical analyses were performed with MedCalc (MedCalc Software), and graphs and plots were performed with Prism (GraphPad Software).

## RESULTS

### Impact of Everolimus on Tumor Xenograft Growth

Tumor growth was monitored over 7 d of treatment with everolimus (Fig. 1A). In the vehicle group, tumor growth was observed from day 0 ( $64 \pm 21$  mm<sup>3</sup>) to day 2 ( $77 \pm 27$  mm<sup>3</sup>,  $P = 0.02$ ) and day 7 ( $91 \pm 20$  mm<sup>3</sup>,  $P = 0.16$ ), with a mean tumor volume doubling time of  $8.7 \pm 3.1$  d. In the everolimus-treated group, tumor volume remained stable from day 0 ( $53 \pm 17$  mm<sup>3</sup>) to day 2 ( $60 \pm 16$  mm<sup>3</sup>,  $P = 0.63$ ) and day 7 ( $54 \pm 16$  mm<sup>3</sup>,  $P = 0.13$ ). No difference in tumor volumes between treated and vehicle mice was seen at day 2 ( $P = 0.16$ ), but a statistically significant difference was observed at day 7 ( $P = 0.005$ ), indicating that this model is responsive to mTOR inhibition.

### Impact of Everolimus on <sup>18</sup>F-FLT Accumulation in SKOV-3 Xenografts

Changes in <sup>18</sup>F-FLT uptake in response to everolimus were measured using PET (Figs. 1B and 1C). At baseline, there was no difference in <sup>18</sup>F-FLT SUVmean between tumors that had been randomized in the vehicle and everolimus groups ( $P = 0.78$ ). In the vehicle group, a nonsignificant increase in tumor <sup>18</sup>F-FLT SUVmean was observed at day 2 ( $+9\% \pm 26\%$ , compared with baseline;  $P = 0.45$ ), followed by a nonsignificant decrease at day 7 ( $-8\% \pm 47\%$ , compared with baseline;  $P = 0.76$ ).

In contrast, <sup>18</sup>F-FLT SUVmean in everolimus-treated mice showed a marked decrease from day 0 to day 2 ( $-33\% \pm 12\%$ , compared with baseline;  $P = 0.003$ ), at a time when no change in tumor volume was detectable between everolimus-treated and vehicle mice. The decrease in <sup>18</sup>F-FLT accumulation in the treated tumors was even more significant at day 7, when SUVmean was reduced by  $66\% \pm 8\%$ , compared with that at baseline ( $P < 0.0001$ ).

A significant difference between <sup>18</sup>F-FLT SUVmean in vehicle and treated tumors was observed at day 2 ( $P =$

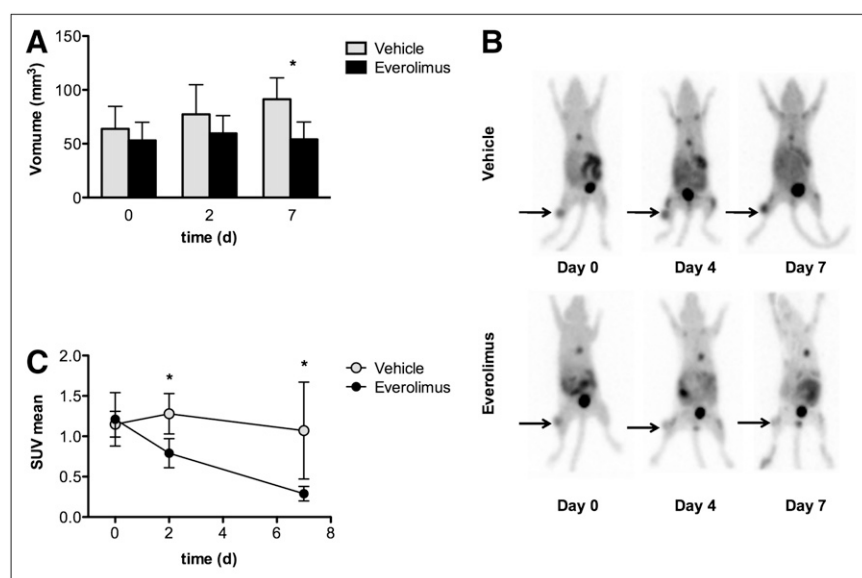


**FIGURE 1.** <sup>18</sup>F-FLT imaging identifies early metabolic changes after treatment by everolimus: tumor volume in everolimus and vehicle groups (A), maximum-intensity projection of representative animal in everolimus and vehicle groups (B), and SUVmean changes (mean  $\pm$  SD) of tumors in mice receiving either everolimus or vehicle (C). \* $P < 0.05$ .

0.0008) and at day 7 ( $P = 0.01$ ). Despite a relatively large SD in the vehicle group at day 7, there was no overlap between SUVmean values in the vehicle and everolimus mice at any time point. We computed SUVmean in order to take into account the whole metabolic behavior of tumors. However, similar results were obtained when using SUVmax, with a significant difference between  $^{18}\text{F}$ -FLT SUVmax in vehicle and treated tumors being observed at day 2 ( $P = 0.0003$ ) and at day 7 ( $P = 0.01$ ) (Supplemental Fig. 1, available online only at <http://jnm.snmjournals.org>).

### Impact of Everolimus Treatment on BrdU Incorporation and pS6 Activity in SKOV-3 Tumors

We used BrdU staining as a biomarker of cell proliferation, and pS6 staining as a specific biomarker of mTOR activity (Fig. 2). In the vehicle group, BrdU incorporation (percentage of stained cells) remained above 5%, without a significant change between baseline, day 2, and day 7. In the everolimus group, BrdU incorporation showed a decrease at day 2 ( $1.9 \pm 1.3$ ,  $P = 0.16$ ) and at day 7 ( $2.9 \pm 1.6$ ,  $P = 0.02$ ), compared with vehicle tumors. The decrease in the mean value for BrdU staining at days 2 and 7 of everolimus treatment represented a 65% and 41% reduction, respectively, compared with vehicle groups.

A significant decrease in pS6 staining was observed in the everolimus-treated tumors at day 2 ( $3.6 \times 10^3 \pm 2.2 \times 10^3$ ,  $P = 0.02$ ) and at day 7 ( $15.5 \times 10^3 \pm 7 \times 10^3$ ,  $P = 0.003$ ), which represented a 98% and 91% reduction of the mean value, respectively, compared with the vehicle groups. In the vehicle group, pS6 activity (optical density) was essentially unchanged during the treatment period.

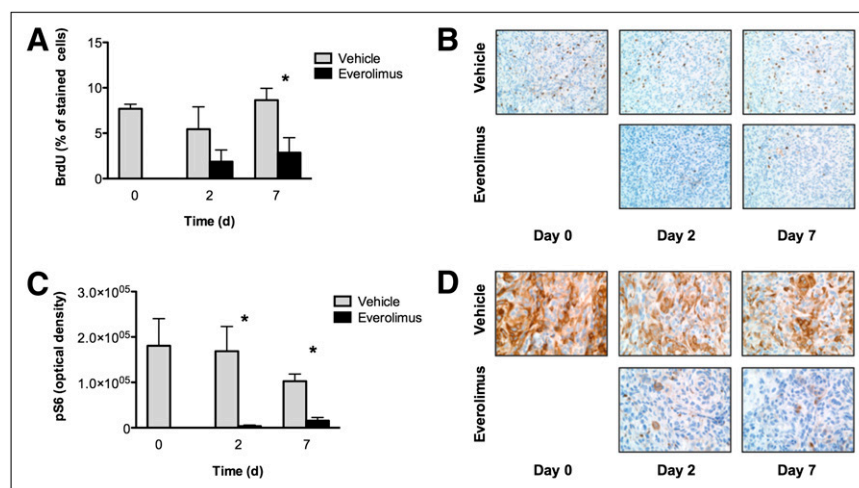
## DISCUSSION

This study demonstrated the ability of  $^{18}\text{F}$ -FLT PET to predict early response to mTOR inhibition in a cisplatin-resistant ovarian cancer model. The results suggest that this technique should be considered for therapeutic response assessment in humans.

Cisplatin resistance is common in ovarian cancer, and the need for second-line therapies is pressing. One such therapeutic option is targeting the phosphoinositide-3-kinase/AKT pathway or its downstream target mTOR, which has an important role in cell growth and proliferation. Despite some promising preclinical results (19), there is a need for improved noninvasive imaging tools for early mTOR inhibition, because  $^{18}\text{F}$ -FDG PET has been shown in a recent clinical study to be ineffective in predicting response to mTOR inhibition by rapamycin in patients with various types of cancer (20). In the current study,  $^{18}\text{F}$ -FLT was chosen because mTOR inhibition is known to cause a decrease in cyclin D1 expression and an increase in p27, leading in turn to a cell-cycle arrest in G1 (21), a state in which thymidine kinase 1 activity is low (19). Consistent with this observation, the significant  $^{18}\text{F}$ -FLT response as early as 2 d after initiation of treatment, with uptake decreasing by 33% at a time when no change in tumor volume was detectable between everolimus-treated and vehicle mice, is expected given that  $^{18}\text{F}$ -FLT is a substrate for thymidine kinase 1. The concordant change in tissue biomarkers of mTOR signaling, including a marked decrease in pS6 activity (98%, compared with vehicle), further suggests that decreased  $^{18}\text{F}$ -FLT uptake is a valid imaging biomarker of abrogation of signaling through this pathway. The reduced incorporation of BrdU—although not reaching statistical significance at day 2, possibly because of the low number of animals used for correlative studies at that time point—was statistically significant at day 7, indicating that a  $^{18}\text{F}$ -FLT PET response may also be imputed as a biomarker of reduced cellular proliferation as a consequence of mTOR inhibition.

The potential implications of the present study are 2-fold. First,  $^{18}\text{F}$ -FLT PET could be used to evaluate novel combination therapies, potentially including a combination of everolimus and conventional chemotherapy agents, with the goal of improving outcomes in platinum-resistant ovarian cancer. The use of  $^{18}\text{F}$ -FLT PET response during lon-

**FIGURE 2.** Changes in  $^{18}\text{F}$ -FLT reflect decrease in cell proliferation and inhibition of mTOR pathway. (A and C) Quantitative immunohistochemistry data (mean  $\pm$  SD) are shown. (B and D) Representative tumor sections for BrdU ( $\times 20$ , B) and pS6 ( $\times 40$ , D) are displayed. \* $P < 0.05$ .





itudinal studies would provide more efficient treatment validation than do tissue biomarker studies, such as immunohistochemistry. A proof-of-concept preclinical study of the utility of molecular imaging in molecularly targeted drug development has recently been published by Cejka et al. (22), who used  $^{18}\text{F}$ -FDG PET to define the optimal dose of the mTOR inhibitor everolimus in a model of human gastric cancer in nude mice. Those authors demonstrated that doses above 5 mg/kg did not further reduce  $^{18}\text{F}$ -FDG uptake. If one assumes that maximal metabolic response reflects abrogation of signaling through the mTOR pathway, it may be possible to titrate the optimal administered dose using molecular imaging and thereby improve the therapeutic index of this therapy by reducing off-target side effects. Although conceptually appealing, the study from Ma et al. (20) suggests that  $^{18}\text{F}$ -FDG may not be the optimal PET probe for evaluation of treatment with mTOR inhibitors in cancer patients. The present study demonstrates that  $^{18}\text{F}$ -FLT imaging is useful in a widely applied ovarian cancer cell line (23,24) and may also be useful for early evaluation of molecularly targeted therapies developed for ovarian cancer.

Although the utility of  $^{18}\text{F}$ -FDG PET for therapeutic response assessment is increasingly recognized, potential limitations have also been demonstrated in preclinical (9,25) and clinical studies (26). Similarly, the role of  $^{18}\text{F}$ -FLT PET for therapeutic monitoring requires further validation and definition of optimal timing in relation to treatment. In particular, it should be recognized that inhibition of proliferation can be a transient phenomenon, especially in the setting of intermittent drug administration, and may be followed by synchronization of cells moving back into cycle. This factor may account for the unexpected rise in  $^{18}\text{F}$ -FLT uptake 7 d after treatment observed in a recent study investigating mTOR inhibition in a murine lymphoma model (27). That study used a single dose of temsirolimus in a tumor model in which cyclin D1 messenger RNA is overexpressed. The increase in  $^{18}\text{F}$ -FLT retention at day 7 likely related to cyclin D1 driving cell-cycle progression of the tumor after release from mTOR inhibition. Accordingly, it will be important to consider the pharmacodynamics of the therapeutic agents being used in designing  $^{18}\text{F}$ -FLT imaging protocols for response assessment.

Despite these challenges, there are clear practical advantages to noninvasive imaging biomarkers that can be used serially in clinical trials of molecularly targeted therapies (2). These include the ability to evaluate multiple lesions throughout the body. Because invasive procedures such as evaluation of Ki67 staining in serial tumor biopsy samples (28) are rarely clinically feasible, they have been replaced by evaluation of biomarkers in surrogate tissues such as skin biopsies or peripheral mononuclear cells (29,30). However, phosphorylation of S6, as shown by clinical data (28), is a marker of target inhibition in normal tissues but not necessarily of tumor response. Moreover, even if serial tumor samples are achievable for tumor pro-

liferation evaluation, they may still be hampered by tumor heterogeneity, whereas  $^{18}\text{F}$ -FLT PET can reliably study cell proliferation within multiple metastases in a single patient. Therefore, findings reported in the present study strongly support the use of  $^{18}\text{F}$ -FLT PET as a complementary tool to predict early response to mTOR inhibition in cancer patients.

## CONCLUSION

In the SKOV-3 model of cisplatin-resistant ovarian cancer, therapeutic response to everolimus, as visualized by  $^{18}\text{F}$ -FLT PET, is closely linked with mTOR inhibition, as demonstrated by reduced S6 phosphorylation and BrdU incorporation. These data support the concept of using  $^{18}\text{F}$ -FLT PET to refine imaging and treatment protocols assessing mTOR inhibitors, and potentially other molecularly targeted therapies, in future clinical trials evaluating treatment of cisplatin-resistant ovarian tumors.

## ACKNOWLEDGMENTS

This work was supported by a fellowship from the Fondation de France and by a grant from the French Ligue contre le cancer, Comité du calvados. The authors thank the animal technologists and research assistants (Rachel Walker, Susan Jackson, Kerry Ardley, Jeannette Valentin, Ekaterina Bogatyreva, and Laura Kirby) from the Centre for Molecular Imaging for caring for the animals, injecting the tracer, and acquiring the SA PET images. Dr. Aide is indebted to Dr. Delphine Lerouge for her continuous support during this work.

## REFERENCES

1. Aebi S, Castiglione M. Epithelial ovarian carcinoma: ESMO clinical recommendations for diagnosis, treatment and follow-up. *Ann Oncol*. 2008;19 (suppl 2):ii14–ii16.
2. Yap TA, Carden CP, Kaye SB. Beyond chemotherapy: targeted therapies in ovarian cancer. *Nat Rev Cancer*. 2009;9:167–181.
3. Dancy JE. Therapeutic targets: MTOR and related pathways. *Cancer Biol Ther*. 2006;5:1065–1073.
4. Fung AS, Wu L, Tannock IF. Concurrent and sequential administration of chemotherapy and the mammalian target of rapamycin inhibitor temsirolimus in human cancer cells and xenografts. *Clin Cancer Res*. 2009;15:5389–5395.
5. Hess G, Herbrecht R, Romaguera J, et al. Phase III study to evaluate temsirolimus compared with investigator's choice therapy for the treatment of relapsed or refractory mantle cell lymphoma. *J Clin Oncol*. 2009;27:3822–3829.
6. Campone M, Levy V, Bourbouloux E, et al. Safety and pharmacokinetics of paclitaxel and the oral mTOR inhibitor everolimus in advanced solid tumours. *Br J Cancer*. 2009;100:315–321.
7. Mabuchi S, Altomare DA, Cheung M, et al. RAD001 inhibits human ovarian cancer cell proliferation, enhances cisplatin-induced apoptosis, and prolongs survival in an ovarian cancer model. *Clin Cancer Res*. 2007;13:4261–4270.
8. Mabuchi S, Altomare DA, Connolly DC, et al. RAD001 (Everolimus) delays tumor onset and progression in a transgenic mouse model of ovarian cancer. *Cancer Res*. 2007;67:2408–2413.
9. Aide N, Poulain L, Briand M, et al. Early evaluation of the effects of chemotherapy with longitudinal FDG small-animal PET in human testicular cancer xenografts: early flare response does not reflect refractory disease. *Eur J Nucl Med Mol Imaging*. 2009;36:396–405.
10. Dorow DS, Cullinane C, Conus N, et al. Multi-tracer small animal PET imaging of the tumour response to the novel pan-Erb-B inhibitor CI-1033. *Eur J Nucl Med Mol Imaging*. 2006;33:441–452.

11. Weber WA. Assessing tumor response to therapy. *J Nucl Med.* 2009;50(suppl 1):1S–10S.
12. Barthel H, Cleij MC, Collingridge DR, et al. 3'-deoxy-3'-[<sup>18</sup>F]fluorothymidine as a new marker for monitoring tumor response to antiproliferative therapy in vivo with positron emission tomography. *Cancer Res.* 2003;63:3791–3798.
13. Machulla HJ, Blocher A, Kuntzsch M, Piert M, Wei R, Grierson JR. Simplified labeling approach for synthesizing 3'-deoxy-3'-([<sup>18</sup>F]fluorothymidine ([<sup>18</sup>F]FLT). *J Radioanal Nucl Chem.* 2000;243:843–846.
14. Huisman MC, Reder S, Weber AW, Ziegler SI, Schwaiger M. Performance evaluation of the Philips MOSAIC small animal PET scanner. *Eur J Nucl Med Mol Imaging.* 2007;34:532–540.
15. Chiang S, Cardi C, Matej S, et al. Clinical validation of fully 3-D versus 2.5-D RAMLA reconstruction on the Philips-ADAC CPET PET scanner. *Nucl Med Commun.* 2004;25:1103–1107.
16. Soret M, Bacharach SL, Buvat I. Partial-volume effect in PET tumor imaging. *J Nucl Med.* 2007;48:932–945.
17. Aide N, Louis MH, Dutoit S, et al. Improvement of semi-quantitative small-animal PET data with recovery coefficients: a phantom and rat study. *Nucl Med Commun.* 2007;28:813–822.
18. Rieux C, Carney R, Lupi D, et al. Analysis of immunohistochemical label of Fos protein in the suprachiasmatic nucleus: comparison of different methods of quantification. *J Biol Rhythms.* 2002;17:121–136.
19. Wei LH, Su H, Hildebrandt JJ, Phelps ME, Czernin J, Weber WA. Changes in tumor metabolism as readout for mammalian target of rapamycin kinase inhibition by rapamycin in glioblastoma. *Clin Cancer Res.* 2008;14:3416–3426.
20. Ma WW, Jacene H, Song D, et al. [<sup>18</sup>F]fluorodeoxyglucose positron emission tomography correlates with Akt pathway activity but is not predictive of clinical outcome during mTOR inhibitor therapy. *J Clin Oncol.* 2009;27:2697–2704.
21. Faivre S, Kroemer G, Raymond E. Current development of mTOR inhibitors as anticancer agents. *Nat Rev Drug Discov.* 2006;5:671–688.
22. Cejka D, Kuntner C, Preusser M, et al. FDG uptake is a surrogate marker for defining the optimal biological dose of the mTOR inhibitor everolimus in vivo. *Br J Cancer.* 2009;100:1739–1745.
23. Devalapally H, Duan Z, Seiden MV, Amiji MM. Modulation of drug resistance in ovarian adenocarcinoma by enhancing intracellular ceramide using tamoxifen-loaded biodegradable polymeric nanoparticles. *Clin Cancer Res.* 2008;14:3193–3203.
24. Ingersoll SB, Patel S, Caballero L, et al. Synergistic cytotoxicity of interferonalpha-2b and interleukin-2 in combination with PBMC against ovarian cancer: development of an experimental model for cellular therapy. *Gynecol Oncol.* 2009;112:192–198.
25. Spaepen K, Stroobants S, Dupont P, et al. [<sup>18</sup>F]FDG PET monitoring of tumour response to chemotherapy: does [<sup>18</sup>F]FDG uptake correlate with the viable tumour cell fraction? *Eur J Nucl Med Mol Imaging.* 2003;30:682–688.
26. Wahl RL, Jacene H, Kasamon Y, Lodge MA. From RECIST to PERCIST: evolving considerations for PET response criteria in solid tumors. *J Nucl Med.* 2009;50(suppl 1):122S–150S.
27. Brepoels L, Stroobants S, Verhoef G, De Groot T, Mortelmans L, De Wolf-Peeters C. [<sup>18</sup>F]-FDG and [<sup>18</sup>F]-FLT uptake early after cyclophosphamide and mTOR inhibition in an experimental lymphoma model. *J Nucl Med.* 2009;50:1102–1109.
28. Tabernero J, Rojo F, Calvo E, et al. Dose- and schedule-dependent inhibition of the mammalian target of rapamycin pathway with everolimus: a phase I tumor pharmacodynamic study in patients with advanced solid tumors. *J Clin Oncol.* 2008;26:1603–1610.
29. Boulay A, Zumstein-Mecker S, Stephan C, et al. Antitumor efficacy of intermittent treatment schedules with the rapamycin derivative RAD001 correlates with prolonged inactivation of ribosomal protein S6 kinase 1 in peripheral blood mononuclear cells. *Cancer Res.* 2004;64:252–261.
30. O'Donnell A, Faivre S, Burris HA III, et al. Phase I pharmacokinetic and pharmacodynamic study of the oral mammalian target of rapamycin inhibitor everolimus in patients with advanced solid tumors. *J Clin Oncol.* 2008;26:1588–1595.



The Journal of  
NUCLEAR MEDICINE

## **$^{18}\text{F}$ -FLT PET as a Surrogate Marker of Drug Efficacy During mTOR Inhibition by Everolimus in a Preclinical Cisplatin-Resistant Ovarian Tumor Model**

Nicolas Aide, Kathryn Kinross, Carleen Cullinane, Peter Roselt, Kelly Waldeck, Oliver Neels, Donna Dorow, Grant McArthur and Rodney J. Hicks

*J Nucl Med.* 2010;51:1559-1564.

Published online: September 16, 2010.

Doi: 10.2967/jnumed.109.073288

---

This article and updated information are available at:

<http://jnm.snmjournals.org/content/51/10/1559>

---

Information about reproducing figures, tables, or other portions of this article can be found online at:

<http://jnm.snmjournals.org/site/misc/permission.xhtml>

Information about subscriptions to JNM can be found at:

<http://jnm.snmjournals.org/site/subscriptions/online.xhtml>

*The Journal of Nuclear Medicine* is published monthly.  
SNMMI | Society of Nuclear Medicine and Molecular Imaging  
1850 Samuel Morse Drive, Reston, VA 20190.  
(Print ISSN: 0161-5505, Online ISSN: 2159-662X)

© Copyright 2010 SNMMI; all rights reserved.

The logo for the Society of Nuclear Medicine and Molecular Imaging (SNMMI) consists of the letters 'S', 'N', 'M', and 'I' arranged in a 2x2 grid. Each letter is white and set within a red square. To the right of this grid, the full name of the society is written in a sans-serif font.  
SOCIETY OF  
NUCLEAR MEDICINE  
AND MOLECULAR IMAGING